ELECTRON-CLOUD UPDATED SIMULATION RESULTS FOR THE PSR, AND RECENT RESULTS FOR THE SNS [*]

M. Pivi and M. A. Furman,[†] LBNL, Berkeley, CA94720, USA

Abstract

Recent simulation results for the main features of the electron cloud in the storage ring of the Spallation Neutron Source (SNS) at Oak Ridge, and updated results for the Proton Storage Ring (PSR) at Los Alamos are presented in this paper. A refined model for the secondary emission process including the so called true secondary, rediffused and backscattered electrons has recently been included in the electron-cloud code.

1 INTRODUCTION

Studies on the possible electron-cloud effect have been initiated at the Spallation Neutron Source (SNS) under construction at the Oak Ridge National Laboratory (ORNL). The electron cloud effect may limit the performance of intense proton storage rings, causing a fast instability that may be responsible for proton losses and collective beam motion above a certain current threshold, accompanied by a large number of electrons. Such a high-intensity instabil-

Table 1: Simulation parameters for the PSR and SNS.

Parameter	Symbol	PSR	SNS
proton beam energy	E, GeV	1.735	1.9
dipole field	B, T	1.2	0.78
bunch population	N_p, $\times 10^{13}$	5	20.5
ring circumference	C, m	90	248
bunch length	b_l, ns	254	760
beam pipe semi-axes	a, b, cm	5,5	10,10
gauss. tr. bunch size	σ_x, σ_y, mm	10, 10	
flat tr. bunch size	r_x, r_y, mm		28, 28
proton loss rate	p_{loss}, $\times 10^{-6}$	4	0.11
proton-electron yield	Y	100	100
No. steps during gap	N_g	100	250
No. kicks/bunch	N_k	1001	5001
max sec. yield	δ_{max}	2.0	2.0
energy at yield max	E_{max}, eV	300	300
yield low energy el.	$\delta(0)$	0.5	0.5

ity which has been observed in the PSR at the Los Alamos National Laboratory (LANL) for more than 13 years, is now recognized to be, although not conclusively proven, an electron-cloud effect. This instability is now believed to be due to the collective coupling between an electron cloud and the proton beam [1, 2]. In this article we present

simulation results for the SNS and for PSR ring obtained with the ECE code that has been developed at LBNL over the past 6 years. In all results presented here, the proton beam is assumed to be a static distribution of given charge and shape moving on its nominal closed orbit, while the electrons are treated fully dynamically. We defer issues like the current instability threshold, growth rate and frequency spectrum to future studies. We compared in [3] our results for the electron current and energy spectrum of the electrons hitting the walls of the chamber against measurements obtained in the PSR by means of dedicated electron probes. From such comparisons we can assess the effects of several important parameters such as the secondary electron yield (SEY) at the walls of the chamber, the proton loss rate and electron yield, etc. Furthermore, we can infer details of the electron cloud in the vicinity of the proton beam, such as the neutralization factor, which is important for a self-consistent treatment of the coupled e-p problem [4].

2 PHYSICAL MODEL

2.1 Sources of electrons

The two main sources of electrons considered for proton storage rings at the SNS and the PSR, are: lost protons hitting the vacuum chamber walls, and secondary emission from electrons hitting the walls (the electron cloud in the vicinity of the stripper foil is not modelled here). Although our code accommodates other sources of electrons, such as residual gas ionization, we have turned them off for the purposes of this article.

2.2 Secondary emission process

The SEY $\delta(E_0)$ and the corresponding emitted-electron energy spectrum $d\delta/dE$ (E_0 =incident electron energy, E = emitted secondary energy) are represented by a detailed model described elsewhere [5]. Its parameters were obtained from detailed fits to the measured SEY of stainless steel [6]. The main SEY parameters are the energy E_{max} at which $\delta(E_0)$ is maximum, and the peak value itself, $\delta_{\text{max}} = \delta(E_{\text{max}})$ (see Table 1). Furthermore, for the results shown below, we do take into account the elastic backscattered and rediffused components of the secondary emitted-electron energy spectrum $d\delta/dE$. The backscattered component typically becomes more important at low incident electron energies. To account for this behavior we have used a fit extrapolated data for copper measured at CERN [7]. The value of $\delta(E_0)$ at incident electron energies E_0 <10eV is an important parameter since it determines the electron survival rate at the end of the gap. This quantity is difficult to measure experimentally, and remains

an uncertainty for the model. However, the decay time of the electron cloud at the end of the beam pulse has been measured in the PSR, see Fig. 1. A long exponential tail seen with 170 ns decay time may imply a high reflectivity for low energy electrons. In Fig. 1, we reproduce the passage of one single PSR beam assuming different values for $\delta(0)$.
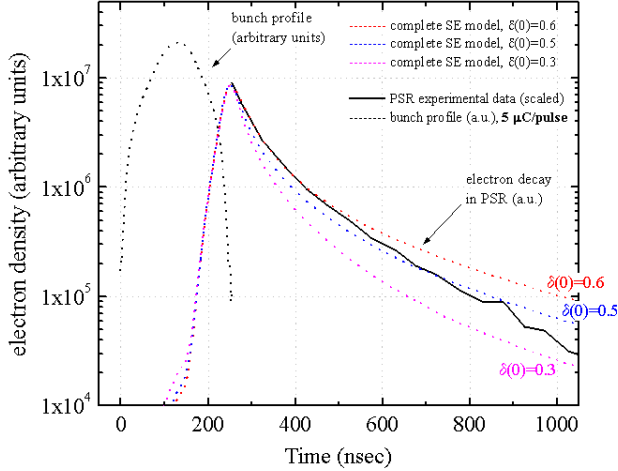

Figure 1: Experimental data from PSR (R. Macek courtesy) and simulated decay time of the electron cloud at end of the beam pulse. Different SEY values for low energy electrons, $\delta(0)$, have been assumed in the simulation.

2.3 Simulation Model

The PSR and the SNS rings store a single proton bunch of length τ_b followed by a gap of length τ_g with a typical current intensity profile shown in Figs. 2 and 3. A Gaussian transverse beam with rms sizes $\sigma_x=\sigma_y=10$ mm, and the actually measured longitudinal intensity profile are assumed for the PSR. The transverse beam distribution for the SNS is assumed to be constant with $r_x=r_y=28$ mm. The vacuum chamber is assumed to be a cylindrical perfectly-conducting pipe. The number of electrons generated by lost protons hitting the vacuum chamber wall is $N_p \times Y \times p_{loss}$ per turn for the whole ring, where Y is the effective electron yield per lost proton, and p_{loss} is the proton loss rate per turn for the whole ring per beam proton. The lost-proton time distribution is proportional to the instantaneous bunch intensity. The electrons are then simulated by macroparticles. The secondary electron mechanism adds to these a variable number of macroparticles, generated according to the SEY model mentioned above. The bunch is divided up into N_k kicks, and the interbunch gap into N_g intermediate steps. The image and space charge forces are computed and applied at each slice in the bunch and each step in the gap. Typical parameter values are shown in Table 1. By comparing the measured and simulated decay time of the electron cloud, shown in Fig. 1, we deduce $\delta(0) \simeq 0.5$, and assume this value for the following simulations presented here.
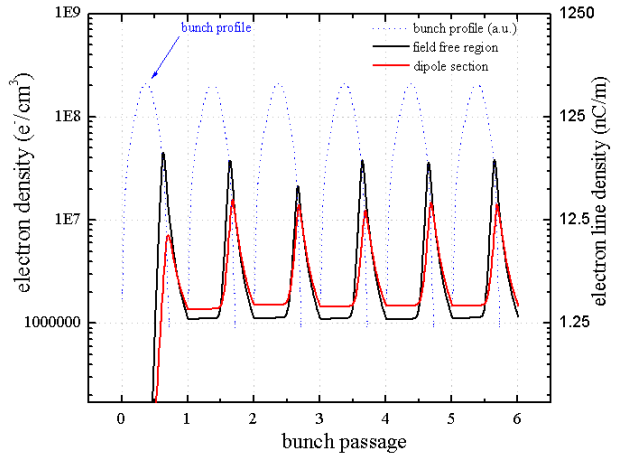

Figure 2: Simulated electron density during the first bunch passages, in a PSR field-free region and a dipole section.
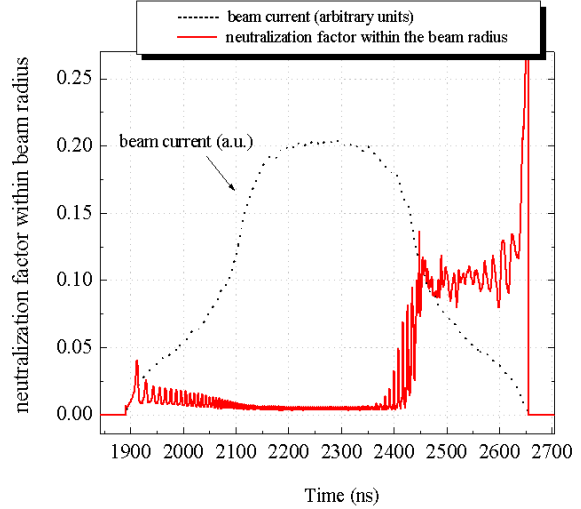

Figure 3: Simulated electron neutralization factor in a SNS field-free region. The fractional charge neutralization computed within the beam radius exceeds 10% at the tail of the bunch.

3 RESULTS AND DISCUSSION

The build-up of the electron cloud in a PSR field-free region and a dipole section during the passage of the beam is shown in Fig. 2. The saturation level in the PSR is reached after few bunch passages, when assuming $\delta_{max} =2$. The estimated peak number of electrons in a field free region is $\sim 4 \times 10^7$ e/cm^3 or 50 nC/m. In particular, when assuming $\delta(0) \simeq 0.5$ the simulated electron density in the PSR increases by a factor ~ 3 relative to the $\delta(0) \simeq 0.1$ case (refer to previous results for PSR, see [3]). These are examples of strong parameter sensitivity that calls for further experimental investigations.

The SNS beam pipe chamber will be coated with TiN. Recent measurements of an *as-received* sample of the TiN coated SNS vacuum chamber, has shown $\delta_{max} =2$ [8]. The build-up of the electron cloud and previous results for the
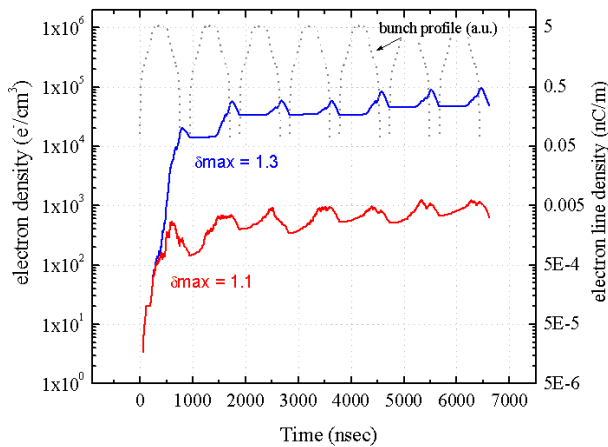
Figure 4: Build-up of the electron cloud in the SNS field-free region assuming a $\delta_{\max}$ =1.3 and 1.1. The electrons gradually increase in number during successive bunch passages until, owing to the space-charge forces, a balance is reached between emitted and absorbed electrons.
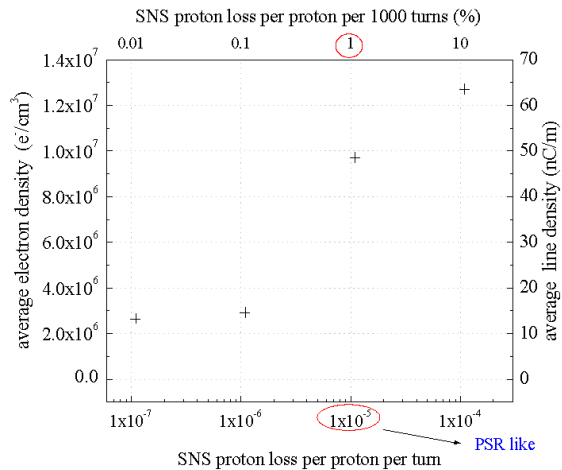

Figure 5: Average electron density (over whole run) in a SNS field free region. Proton losses of 10^{-7} protons loss per proton per turn are expected in the SNS ring. Secondary electron yield $\delta_{\max}$=2.

SNS field-free region and dipole section for $\delta_{\max}$ =2 are shown in [1]. Due to the large electron multiplication, we have used a very low initial number of macroparticles per bunch passage, leading to significant fluctuations in the turn-by-turn electron density. Simulation results for the SNS obtained with a different code [10] show a qualitative agreement with our results, although they yield a lower estimated electron density at this SEY value. The neutralization factor, ratio e/p, computed within the beam radius region, is shown in Fig. 3. For $\delta_{\max}$=1.3 and 1.1, we were able to increase significantly the number of macroparticles, leading to better statistics. The build-up of the electron cloud during the first few bunch passages is shown in Fig.4. The simulated electron density (averaged over the whole run) in a SNS field free region is shown in Fig. 5, when assuming $\delta_{\max}$=2. Proton losses corresponding to 10^{-7} protons loss per proton per turn are expected in the SNS ring.

4   CONCLUSION

We present updated electron cloud simulations for PSR and preliminary simulations for the SNS. When considering proton losses of 10^{-7}, an average density 10 nC/m with peaks of $\geq$ 150 nC/m may be reached in an SNS field-free region. The related neutralization factor exceeds 10% at the tail of the beam pulse. High electron density may lead to a significant tune shift and consequent high proton losses, see [3]. Due to a large unexpected electron multiplication in the case of the SNS, we have used a low number of macroparticles per bunch passage.

5   ACKNOWLEDGEMENTS

We are particularly grateful to our colleagues of the PSR Instability Studies Program for many stimulating discus-

sions, especially to R. Macek for discussions and for providing us the experimental data. We are grateful to NERSC for supercomputer support.

6   REFERENCES

[1] For an updated summary and links on electron cloud studies, see: *Mini-Workshop on Electron-Cloud Simulations for Proton and Positron Beams* ECLOUD02, CERN, 15-18 April 2002, http://slap.cern.ch/collective/ecloud02/, or also Physical Review Special Topic (PRST) - Accelerator and Beams (AB) ECLOUD02 Special Collection Edition, future publication.

[2] R. Macek ECLOUD02 proceedings, see ref. [1].

[3] M. Furman and M. Pivi, Proc. PAC01, Chicago, IL, p. 708, and also ECLOUD02 proceedings, see ref. [1].

[4] For an updated on the self consistent treatment of the instability see, for example ECLOUD02 proceedings, see ref. [1].

[5] M. A. Furman and M. Pivi *Microscopic Probabilistic Model for the Simulation of the Secondary Electron Emission*, LBNL-49711, CBP Note-415, to be submitted to Physical Review Special Topics, May 2002.

[6] R. Kirby, private communication.

[7] V. Baglin, I. Collins, B. Henrist, N. Hilleret, G. Vorlaufer, *A Summary of Main Experimental Results Concerning the Secondary Electron Emission of Copper*, LHC-Project-Report-472.

[8] M. Blaskiewicz, private communication, May 2002.

[9] T. Toyama, K. Ohmi, *Study for ep Instability in High Intensity Proton Ring*, these proceedings.

[10] M. Blaskiewicz *Electron Cloud in the PSR and SNS* these proceedings.

7 DISCLAIMER